

THE 3 μm SPECTRUM OF JUPITER'S IRREGULAR SATELLITE HIMALIA

M. E. BROWN¹ AND A. R. RHODEN²

¹ Division of Geological and Planetary Sciences, California Institute of Technology, Pasadena, CA 91125, USA; mbrown@caltech.edu

² Johns Hopkins University Applied Physics Laboratory, Laurel, MD 20723, USA; Alyssa.Rhoden@jhuapl.edu

Received 2014 August 6; accepted 2014 September 3; published 2014 September 19

ABSTRACT

We present a medium resolution spectrum of Jupiter's irregular satellite Himalia covering the critical 3 μm spectral region. The spectrum shows no evidence for aqueously altered phyllosilicates, as had been suggested from the tentative detection of a 0.7 μm absorption, but instead shows a spectrum strikingly similar to the C/CF type asteroid 52 Europa. 52 Europa is the prototype of a class of asteroids generally situated in the outer asteroid belt between less distant asteroids which show evidence for aqueous alteration and more distant asteroids which show evidence for water ice. The spectral match between Himalia and this group of asteroids is surprising and difficult to reconcile with models of the origin of the irregular satellites.

Key words: planets and satellites: composition – planets and satellites: formation – planets and satellites: individual (Himalia)

Online-only material: color figures

1. INTRODUCTION

The origin of the irregular satellites of the giant planets—small satellites in distant, eccentric, and inclined orbits about their parent body—remains unclear. Early work suggested that the objects were captured from previously heliocentric orbits by gas drag (Pollack et al. 1979) or collisions (Colombo & Franklin 1971), while more recent ideas have suggested that the irregular satellites were captured from the outer solar system during the final stages of a giant planet dynamical instability which violently rearranged the solar system (Nesvorný et al. 2007, 2014).

The surface compositions of the irregular satellites have often been used to attempt to understand the origins of these bodies. Unfortunately, the information we have on their compositions is sparse. Visible through near-infrared photometry and spectroscopy show generally featureless spectra with flat to slightly red slopes in the optical and slightly red slopes in the near-infrared (Rettig et al. 2001; Grav et al. 2003; Grav & Holman 2004; Vilas et al. 2006). By analogy to asteroids, these characteristics often lead to these satellites to be referred to as C-type or P/D-type objects, with the implication of a common origin between the irregular satellites and these asteroids, though the genetic connection is far from clear.

Himalia is the largest of the Jovian irregular satellites and the largest member of the prograde group of Jovian irregular satellites, which are all thought to be part of a single collisional family. The spectra of Himalia and most of the other members of its family show a distinct broad absorption feature from the visible to the near infrared with a center around 1 μm (Grav et al. 2003; Grav & Holman 2004). Detection of a 0.7 μm absorption band has been reported from some data, but not from others (Jarvis et al. 2000; Vilas et al. 2006). Such a feature, if actually present, may result from oxidized iron in phyllosilicate minerals potentially caused by aqueous processing on these bodies.

In a study of dark asteroids in the outer belt, Takir & Emery (2012) found that all asteroids that they observed which have clear 0.7 μm absorption bands showed a sharp 3 μm absorption feature consistent with hydroxyl-group absorption in

phyllosilicates. A spectrum of Himalia obtained from a distant encounter of the *Cassini* spacecraft shows the possibility of an absorption at 3 μm , but the low signal-to-noise and low spectral resolution prohibits clear interpretation (Chamberlain & Brown 2004).

Here we present a high resolution moderate signal-to-noise spectrum of Himalia from 2 to 4 μm obtained from the Keck Observatory. The spectrum shows unambiguous evidence of an absorption at 3 μm . Below we identify and model the absorption feature and discuss the possible surface composition of Himalia. Finally we discuss the implication for the origin of the parent body of Himalia and for the irregular satellites.

2. OBSERVATIONS

We observed Himalia on the nights of 2013 November 26 and 28 using the facility moderate resolution near infrared spectrograph NIRSPEC (McLean et al. 1998). NIRSPEC in its current configuration covers a limited spectral range, so to cover the full 2.2–3.8 μm region requires two spectral settings, one covering 2.25–3.10 μm and the other covering 2.96–3.81 μm . In each spectral setting, we nodded the target between two positions on the 0.57 arcsec wide slit. For the shorter wavelength setting integration times were 7.5 s with 30 coadds, and we obtained 12 such spectra each night for a total integration time of 45 minutes. For the longer wavelengths, with higher thermal emission, integration times were 1 s with 150 coadds, and we obtained 24 such spectra the first night and 36 the second, for a total integration time of 150 minutes. We obtained identical spectral of G 91-3, a G2V star with $V = 7.4$ a distance 3.2 deg from Himalia. All Himalia spectra were obtained at airmasses between 1.0 and 1.1, and the spectra of the calibrator star were obtained within 0.1 of the same airmass, and immediately preceding or following the Himalia observation.

To obtain calibrated data from the raw spectra, we first subtract each temporally adjacent pair of images in which the spectra are in two separate spatial positions. This subtraction removes the bulk of the telescope and sky emission, leaving a positive and negative spectrum of the source along with any

small sky or telescope changes that occurred between the two spectra. A point-source spectrum projects as a curve onto the detector, and sky emission lines which fill the slit have variable curvature as a function of wavelength. We use measurements of the positions of the bright calibrator star in the two slit positions and measurements of the positions of sky lines in the longer target exposures to create a template allowing us to map the non-rectilinear geometry of the data onto a new rectilinear grid with the spatial dimension along one axis and the wavelength along the other. We then use this template to remap the spectral pairs onto a rectilinear grid. We find the spatial profile of the spectrum by taking a median along the spectral dimension. Typical FWHM in the spatial dimension is 0.9 arcsec. To obtain the flux at each wavelength we fit the expected spatial profile plus a linear offset to 50 pixels on either side of the maximum of the spatial profile. Bad pixels are flagged and ignored in the fit. This procedure removes any residual sky lines and also corrects for most of the thermal drift of the telescope which can be important beyond about $3.5 \mu\text{m}$. Examining the final spectral images individually, we found, however, that for about 20% of the longer wavelength spectra the pair subtracted poorly, leaving large residuals in the spatial dimension, which are most likely caused by thermal changes in the telescope. We discard those data affected by this problem, leaving a final total integration time for the longer wavelength data of 122.5 minutes. The individual spectra are summed with 5σ and greater outliers from the mean at each wavelength removed. An identical procedure is performed for the stellar calibration spectra, and the target spectrum is divided by the stellar spectrum to obtain a relatively calibrated spectrum. The shorter and longer wavelength spectra are scaled such that the median of the data in the overlap region is identical. Wavelength calibration is obtained by matching the spectrum of the calibrator to a theoretical transmission spectrum of the terrestrial atmosphere.

The original data has a spectral resolution of approximately $R/\Delta R \sim 2000$. To increase the signal-to-noise per resolution element, we convolve the spectrum with a Gaussian filter with a FWHM of 8 pixels, for a final 2 pixel resolution of ~ 500 . To achieve the strongest possible constraint on any $3 \mu\text{m}$ absorption, we separately calculate reflectances in windows centered at 2.828 and $2.857 \mu\text{m}$, which present small transparent regions through the atmosphere surrounded by strong telluric absorption. The final calibrated spectrum is shown in Figure 1. While the spectrum is only calibrated in terms of relative reflectance, we estimate the reflectance by assuming a value of for the *K*-band albedo of 0.08 after Chamberlain & Brown (2004).

3. RESULTS

The spectrum of Himalia shows a clear sign of absorption in the $3 \mu\text{m}$ region (Figure 1). Because of the report of the $0.7 \mu\text{m}$ absorption feature and its associated with hydrated silicates, we first attempt to model the $3 \mu\text{m}$ spectrum of Himalia with typical hydrated silicate spectra. These spectra have peak absorption in the unobserved $2.5\text{--}2.8 \mu\text{m}$ region and their reflectivities sharply rise longward of $2.8 \mu\text{m}$ (see the Takir & Emery 2012 “sharp” spectral group). In Figure 1 we compare Himalia to a spectrum of a CM chondrite measured under dry conditions (Takir et al. 2013) whose spectrum is consistent with cronstedtite—a phyllosilicate which is a major constituent of CM chondrites—scaled to match the continuum level at wavelengths shortward of $2.5 \mu\text{m}$. While the match beyond $3.0 \mu\text{m}$ is adequate, shortward of $3.0 \mu\text{m}$ the spectrum

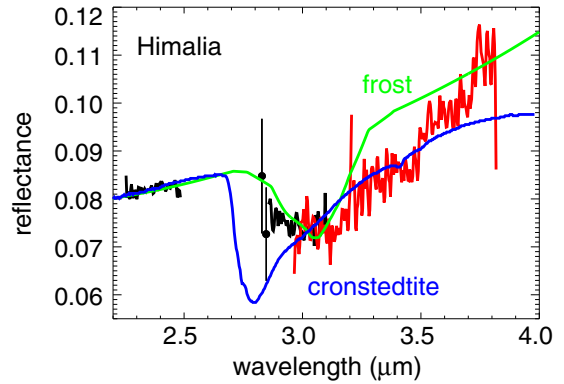


Figure 1. Spectrum of Himalia from 2.2 to $3.8 \mu\text{m}$. The shorter and longer wavelength NIRSPEC settings are shown as black and red, respectively. The spectrum is compared to a CM chondrite with a spectrum consistent with cronstedtite (blue)—a commonly occurring meteoritic phyllosilicate—and to a model of fine grained water ice frost overlying dark grains (green). Neither material provides a satisfactory match to the spectrum of Himalia.

(A color version of this figure is available in the online journal.)

of Himalia turns upward rather than continuing downward like a typical phyllosilicate. The spectrum of Himalia fits neither this particular mineral nor the general characteristics of the Takir & Emery (2012) “sharp” class of dark asteroids with $0.7 \mu\text{m}$ absorptions and sharply rising spectra from $2.8 \mu\text{m}$.

The absorption centered at approximately $3.0 \mu\text{m}$ in the spectrum of Himalia appears more similar to water ice than to OH absorption. To examine this possibility we construct a Shkuratov model (Shkuratov et al. 1999) of dark grains covered with fine grained ice, following the prescription of Rivkin & Emery (2010). In our model the dark grains have optical constants chosen to match the overall albedo level of the continuum and the ice is a fine-grained frost with a volume fraction of 1.5% (chosen to match the depth of the absorption) coating the dark grains. Water ice optical constants are obtained from Mastrapa et al. (2009). This model provides an adequate match to the $2.8\text{--}3.1 \mu\text{m}$ range of the data, but Himalia shows significantly more absorption out to $3.6 \mu\text{m}$ which cannot be accounted for by water ice (Figure 1).

A search of all available libraries of reflectance spectra reveals no materials which can match the spectrum of Himalia. A closer match can be obtained, however, by comparing the spectrum of Himalia with those of dark main belt asteroids. The spectrum of asteroid 24 Themis, for example, similarly contains a water ice-like feature at $\sim 3.1 \mu\text{m}$ followed by continued absorption out to $3.6 \mu\text{m}$ (Campins et al. 2010; Rivkin & Emery 2010), but a close comparison of the two spectra shows that the peak of absorption in the spectrum of Himalia is shifted by $\sim 0.05 \mu\text{m}$ compared to that of 24 Themis. An excellent match to the spectrum of Himalia comes, however, from the spectrum of the CF type asteroid 52 Europa obtained by Takir & Emery (2012). In Figure 2 we compare the spectrum of Himalia to a model where we have taken the spectrum of 52 Europa and allowed the spectral slope and depth of absorption to be free parameters in a fit to the data. The best fit gives a spectrum with a $2.4\text{--}3.7 \mu\text{m}$ slope 23% redder than that of 52 Europa and an absorption 70% deeper. The resulting spectrum is nearly indistinguishable from that of Himalia. Moreover, the overall shape of the visible through and $2 \mu\text{m}$ spectrum with a broad absorption centered at $\sim 1.2 \mu\text{m}$ appears very similar to the available broadband photometry of Himalia (Grav et al. 2003; Grav & Holman 2004). However, the spectra of the Europa-like

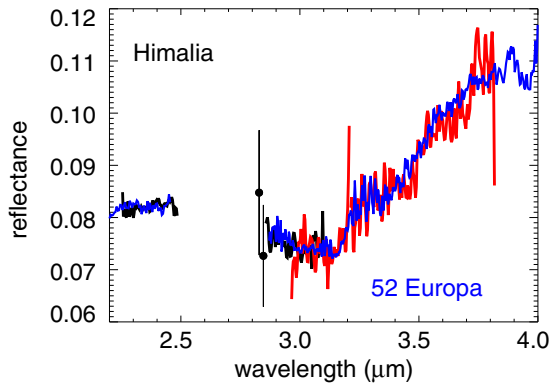


Figure 2. Spectrum of Himalia compared to the spectrum of the 52 Europa (blue), the prototype of the Takir & Emery (2012) “Europa-like” spectrum. The match is excellent, as is the match to the shorter wavelength portions of the spectrum. The surface composition of the Europa-like group is unknown, but the other members are all situated in the middle of the asteroid belt.

(A color version of this figure is available in the online journal.)

group of asteroids lack any $0.7\ \mu\text{m}$ absorption feature. Based on the otherwise strong match between Himalia and 52 Europa and the strong correlation between $0.7\ \mu\text{m}$ absorption and the appearance of the sharp OH-like absorption at $3\ \mu\text{m}$ not seen on Himalia, we suspect that no actual $0.7\ \mu\text{m}$ absorption on Himalia is present. This suspicion requires observational confirmation. We conclude that had Himalia been a dark asteroid in the survey of Takir & Emery (2012) it would have clearly fit into the group of Europa-type spectra that includes 52 Europa, 31 Euphrosyne, and 451 Patientia.

4. DISCUSSION

The Jupiter irregular satellite Himalia has a $0.5\text{--}3.8\ \mu\text{m}$ spectrum which fits into one of the four spectral categories identified by Takir & Emery (2012) for dark asteroids in the outer asteroid belt. Himalia appears to have a “52 Europa-like” spectrum. The 3 known asteroids with Europa-like spectra are all in the middle part of the asteroid belt, with semimajor axes between 3.1 and 3.2 AU. The majority of the asteroids surveyed with semimajor axes inward of 3.1 AU had evidence for OH bearing phyllosilicates suggestive of processing by liquid water, while the majority of more distant asteroids had rounded $3\ \mu\text{m}$ spectra which appear to be evidence for the continued presence of water ice rather than hydrated silicates. The surface composition of the asteroids with Europa-like spectra is unclear, though their semimajor axes between the regions of the asteroid belt containing the other two types of spectra suggests that they might be some sort of transition objects.

In this context, the similarity of the spectrum of Himalia with those of the Europa-like group is surprising. If Himalia is genetically related to the dark asteroids it might be expected to be like the most distant of those asteroids, which tend to have rounded, ice-like spectra. Alternatively, if the Jovian irregular satellites are instead derived from the same source as the Kuiper belt objects, the surface spectral similarity with objects in the

mid-section of the asteroid belt points to either compositional or surface similarities between these populations or both.

Further insight into the origin of this spectral similarity will come from the discovery of additional objects with Europa-like spectra in the asteroid belt. With only three objects currently known the true extent of their distribution is unclear. Additional insight could also come from similar observations of Jupiter trojan asteroids. In the context of the Nice model, these objects are also thought to derive from the Kuiper belt source region, and they are currently situated at the same semi-major axis and thus have the same thermal and irradiation environment as the Jovian irregular satellites. An extensive visible to near-infrared survey of these objects found none with the broad $\sim 1\ \mu\text{m}$ absorption seen on Himalia, so it is clear that these objects are not spectrally identical to Himalia. Nonetheless, examining their spectral morphology at $3\ \mu\text{m}$ should provide important insight into the genetic links and the surface processing of the varied populations of the middle part of the solar system.

We thank Andy Rivkin and Josh Emery for illuminating conversations about the nature of $3\ \mu\text{m}$ absorptions in dark asteroids and for providing the spectra of Themis and Europa. Driss Takir made excellent suggestions which improved the Letter. This research was supported by grant NNX09AB49G from the NASA Planetary Astronomy Program. A. Rhoden was partially supported through an appointment to the NASA Postdoctoral Program at the NASA Goddard Space Flight Center, administered by Oak Ridge Associated Universities. The data presented herein were obtained at the W. M. Keck Observatory, which is operated as a scientific partnership among the California Institute of Technology, the University of California and the National Aeronautics and Space Administration. The Observatory was made possible by the generous financial support of the W. M. Keck Foundation. The authors wish to recognize and acknowledge the very significant cultural role and reverence that the summit of Mauna Kea has always had within the indigenous Hawaiian community. We are most fortunate to have the opportunity to conduct observations from this mountain.

REFERENCES

- Campins, H., Hargrove, K., Pinilla-Alonso, N., et al. 2010, *Natur*, **464**, 1320
 Chamberlain, M. A., & Brown, R. H. 2004, *Icar*, **172**, 163
 Colombo, G., & Franklin, F. A. 1971, *Icar*, **15**, 186
 Grav, T., & Holman, M. J. 2004, *ApJL*, **605**, L141
 Grav, T., Holman, M. J., Gladman, B. J., & Aksnes, K. 2003, *Icar*, **166**, 33
 Jarvis, K. S., Vilas, F., Larson, S. M., & Gaffey, M. J. 2000, *Icar*, **145**, 445
 Mastrapa, R. M., Sandford, S. A., Roush, T. L., Cruikshank, D. P., & Dalle Ore, C. M. 2009, *ApJ*, **701**, 1347
 McLean, I. S., Becklin, E. E., Bendiksen, O., et al. 1998, *Proc. SPIE*, **3354**, 566
 Nesvorný, D., Vokrouhlický, D., & Deienno, R. 2014, *ApJ*, **784**, 22
 Nesvorný, D., Vokrouhlický, D., & Morbidelli, A. 2007, *AJ*, **133**, 1962
 Pollack, J. B., Burns, J. A., & Tauber, M. E. 1979, *Icar*, **37**, 587
 Rettig, T. W., Walsh, K., & Consolmagno, G. 2001, *Icar*, **154**, 313
 Rivkin, A. S., & Emery, J. P. 2010, *Natur*, **464**, 1322
 Shkuratov, Y., Starukhina, L., Hoffmann, H., & Arnold, G. 1999, *Icar*, **137**, 235
 Takir, D., & Emery, J. P. 2012, *Icar*, **219**, 641
 Takir, D., Emery, J. P., McSween, H. Y., et al. 2013, *M&PS*, **48**, 1618
 Vilas, F., Lederer, S. M., Gill, S. L., Jarvis, K. S., & Thomas-Osip, J. E. 2006, *Icar*, **180**, 453